Multiscale Physical and Biological Dynamics in the Philippine Archipelago

Predictions and Processes
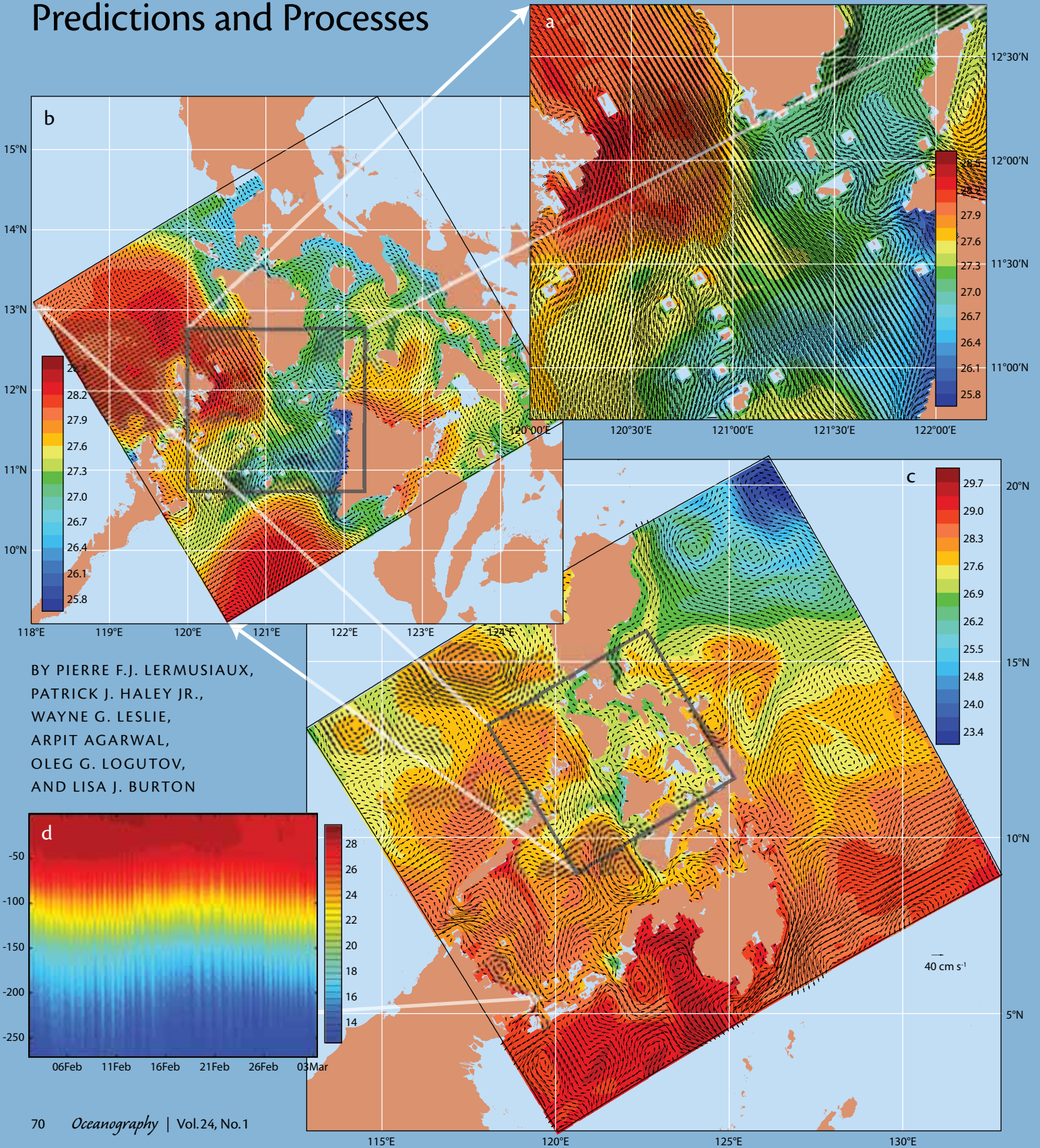
BY PIERRE F.J. LERMUSIAUX,
PATRICK J. HALEY JR.,
WAYNE G. LESLIE,
ARPIT AGARWAL,
OLEG G. LOGUTOV,
AND LISA J. BURTON

ABSTRACT. The Philippine Archipelago is remarkable because of its complex geometry, with multiple islands and passages, and its multiscale dynamics, from the large-scale open-ocean and atmospheric forcing, to the strong tides and internal waves in narrow straits and at steep shelfbreaks. We employ our multiresolution modeling system to predict and study multiscale dynamics in the region, without the use of any synoptic in situ data, so as to evaluate modeling capabilities when only sparse remotely sensed sea surface height is available for assimilation. We focus on the February to March 2009 period, compare our simulation results to ocean observations, and utilize our simulations to quantify and discover oceanic features in the region. The findings include: the physical drivers for the biogeochemical features; the diverse circulation features in each sub-sea and their variations on multiple scales; the flow fields within the major straits and their variability; the transports to and from the Sulu Sea and the corresponding balances; and finally, the multiscale mechanisms involved in the formation of the deep Sulu Sea water.

INTRODUCTION

The Philippine Archipelago is a fascinating multiscale ocean region. Its geometry is very complex, with multiple straits, islands, steep shelf-breaks, and coastal features, leading to partially interconnected seas and basins (Figure 1). At depth, bathymetric barriers form the boundaries of a number of semi-enclosed seas. On the east, the western Pacific, including the North Equatorial Current, Kuroshio, and Mindanao Current dynamically force these multiply connected domains. On the north-northwest, they are forced by the South China Sea and its coastal currents, eddies, and jets. The interactions of these forcings at lateral boundaries with complex geometry drive abundant flow features with varied temporal and spatial scales (Broecker et al., 1986; Metzger and Hurlburt, 1996; Gordon et al., 2011) and multiple feedbacks to the lateral forcing seas. Several

surface and subsurface water masses are advected to the archipelago, where they interact and every so often mix to form new water properties. Due to Earth's rotation, and the ocean's stratification and complex bathymetry, mesoscale features are created, often with spatially inhomogeneous Rossby radii of deformation. The surface atmospheric fluxes are also multiscale, including interannual variations, monsoon regimes, weather events, and topographic wind jets (May et al., 2011; Pullen et al., 2011). Bottom forcing also occurs, for example, in deep waters that are known to be affected by hydrothermal vents (e.g., Gamo et al., 2007). Finally, and as importantly, barotropic tides, often out of phase in the different basins (Logutov, 2008), strongly affect flows, especially in shallower regions and straits. Due to the area's variable stratification, rotation, and steep topographies, they drive a wealth of internal tides, waves, and solitons, some

of which are known to be among the strongest in the world (e.g., Apel et al., 1985). The purpose of the present study is to describe and reveal such regional ocean features as estimated by a multi-resolution, tidally driven ocean model for the February and March 2009 period, without any in situ data assimilation. Our ocean science focus is on biogeo-chemical fields and circulation features, transport balances for the Sulu Sea and flow fields in the corresponding straits, and, finally, formation mechanisms for the deep Sulu Sea water.

The goals of the Philippine Straits Dynamics Experiment (PhilEx; Gordon, 2009; Lermusiaux et al., 2009; Gordon et al., 2011) were to enhance our understanding of physical and biogeo-chemical processes and features arising in and around straits, and to improve our capability to predict the spatial and temporal variability of these regions. A specific objective of the modeling research was to evaluate the capability of tuned modeling systems to estimate the circulation features and processes using only historical data sets for initialization and only remotely sensed data for assimilation, for example, satellite sea surface temperature (SST), height (SSH), and color (SSC). The applied motivation of this approach is to simulate the very frequent operational situation where no synoptic in situ data can be collected, and remotely sensed data are the only synoptic information available. The scientific motivation is to evaluate the intrinsic capabilities of models, specifically to determine if some dynamics can be simulated without using any synoptic in situ data.

For our PhilEx simulations, we employ the MIT Multidisciplinary

Opposite page. MIT Multidisciplinary Simulation, Estimation, and Assimilation System (MSEAS) estimates of: (a-c) 25-m temperature at 0430Z on February 17, 2009 from three implicit two-way nested simulations at 1-km, 3-km, and 9-km resolutions, and (d) a time series of temperature profiles at the Sulu Sea entrance to Sibutu Passage. Features are simulated at multiple scales, including the North Equatorial Current, mesoscale eddies, jets, filaments, and internal tides and waves.
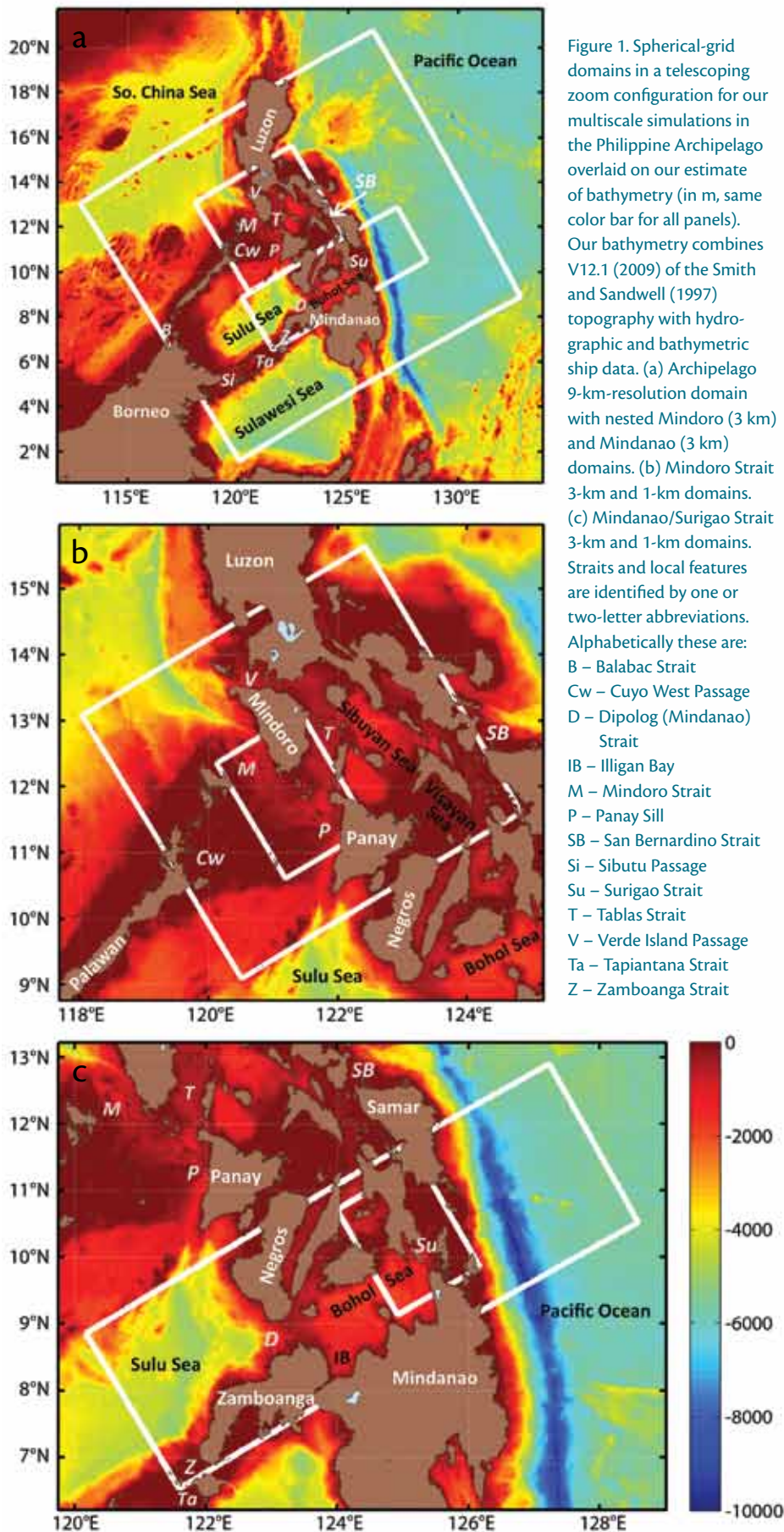
Figure 1. Spherical-grid domains in a telescoping zoom configuration for our multiscale simulations in the Philippine Archipelago overlaid on our estimate of bathymetry (in m, same color bar for all panels). Our bathymetry combines V12.1 (2009) of the Smith and Sandwell (1997) topography with hydrographic and bathymetric ship data. (a) Archipelago 9-km-resolution domain with nested Mindoro (3 km) and Mindanao (3 km) domains. (b) Mindoro Strait 3-km and 1-km domains. (c) Mindanao/Surigao Strait 3-km and 1-km domains. Straits and local features are identified by one or two-letter abbreviations. Alphabetically these are:
B – Balabac Strait
Cw – Cuyo West Passage
D – Dipolog (Mindanao) Strait
IB – Illigan Bay
M – Mindoro Strait
P – Panay Sill
SB – San Bernardino Strait
Si – Sibutu Passage
Su – Surigao Strait
T – Tablas Strait
V – Verde Island Passage
Ta – Tapiantana Strait
Z – Zamboanga Strait

Simulation, Estimation, and Assimilation System (MSEAS Group, 2010). It includes a free-surface hydrostatic primitive-equation physical ocean model developed for multiscale dynamics, resolving very shallow regions with strong tides, steep bathymetries, and the deep ocean. The system is capable of multiresolution simulations over complex geometries with implicit schemes for telescoping nesting (Haley and Lermusiaux, 2010) and has an option for stochastic subgrid-scale representations (Lermusiaux, 2006). The physical model is coupled to multiple biological models (Besiktepe et al., 2003; Tian et al., 2004) and acoustic models (Lam et al., 2009; Lermusiaux et al., 2010). The ocean physics is forced with high-resolution barotropic tides, estimated using nested coastal inversions (Logutov and Lermusiaux, 2008). Due to the complex multiconnected sea domains, all ocean fields are initialized here with new objective mapping schemes developed specifically for PhilEx, using fast marching methods (Agarwal, 2009; Agarwal and Lermusiaux, 2010). SST is only used in the initial conditions. There is no in situ data assimilation (Lermusiaux, 1999, 2002, 2007; Lermusiaux et al., 2000); the only synoptic data used are the sparse satellite SSH observations, providing weak corrections every four days to a week.

During the two-month Intensive Observational Period of February to March 2009 (IOP-09), the MSEAS system was employed in real time, issuing daily physical-biological forecasts. Dynamical descriptions and adaptive sampling guidance were also provided every three to four days

(Lermusiaux et al., 2009). Fields were compared to data sets from ships and gliders when available.

The present work is partly inspired by our experience in coastal regions with complex geometries (Haley and Lermusiaux, 2010), especially with steep shelfbreaks and straits such as the Sicily Strait (Lermusiaux, 1999; Lermusiaux and Robinson, 2001), Massachusetts Bay and Stellwagen Bank (Besiktepe et al., 2003), Middle Atlantic Bight shelfbreak (Lermusiaux, 1999), Monterey Bay shelfbreak (Haley et al., 2009), and Taiwan region shelfbreak (Lermusiaux et al., 2010). However, in addition to being at least an order of magnitude more complex, in a large part due to the very intricate geometry and multiscale flows, a major difference between the present simulations and the earlier studies is that very little was known about the dynamics in the region prior to the three PhilEx expeditions (Gordon et al., 2011). For example, it is interesting to note that for the month of February, there is not one single conductivity-temperature-depth (CTD) profile recorded for the Sulu Sea in the National Oceanographic Data Center (NODC) World Ocean Atlas 2005 (WOA05, Antonov et al., 2006; Locarnini et al., 2006), although this database goes back for more than the past 100 years.

In the following, we first outline our multiresolution simulation approach and its parameters. We then present selected real-time multiscale forecasting results,

focusing on their most novel components: biogeochemical ocean predictions with region-specific biological state initializations and multiresolution tidal predictions. We then describe a subset of our re-analysis modeling results and compare them to ocean observations. We report the major circulation features estimated and discuss our estimates of transports to and from the Sulu Sea as well as the flow fields in the corresponding straits. Finally, we examine the multiscale formation mechanisms for the deep Sulu Sea water.

SIMULATION METHODOLOGIES AND PARAMETERS
Multiresolution Simulations

The MSEAS ocean modeling system (Haley and Lermusiaux, 2010) solves the oceanic primitive equations (PEs) with a nonlinear free surface and tidal forcing. It employs a conservative structured finite-volume grid with time-dependent discretizations and two-way nesting for multiresolution, telescoping domains. The resulting schemes are suitable for realistic data-driven multi-scale simulations over deep seas to very shallow coastal regions with strong tidal forcing. We employ second-order temporal and spatial discretizations that account for the time variations in the finite volumes and nonlinear free surface, and include spherical coordinates and generalized vertical grids. Along with the PE model are modules for data assimilation, atmospheric and

tidal forcing, parameterizations for river input and subgrid-scale processes, feature models (Gangopadhyay et al., 2003), and a suite of coupled biological (NPZ) models. In the present IOP-09 multiresolution simulations, we use the two-way nesting scheme fully implicit in space and time (i.e., such that within each time step, updated field values are exchanged across scales and nested domains as soon as they become available). This method differs from explicit nesting schemes that exchange coarse and fine domain fields only at the start of a discrete time integration or time step. Our nested simulations also use different parameterizations for the subgrid-scale physics in each of the nested domains. Numerical and theoretical analysis of these schemes can be found in Haley and Lermusiaux (2010).

Modeling Domains and Bathymetry

For the PhilEx region, we employ spherical coordinates and six two-way nested domains in telescoping setups (Figure 1), ranging from a 3267 x 3429 km regional domain at 27-km resolution (not depicted) down to a pair of roughly 170 x 220 km strait domains with high (1-km) resolution. The simulations shown next are for the February to March 2009 period, focusing on the 1656 x 1503 km Philippine Archipelago domain (9-km resolution), the 552 x 519 km Mindoro Strait domain (3-km resolution), and the 895 x 303 km Mindanao domain (3-km resolution). All domains have 70 vertical levels arranged in a double-sigma configuration, optimized for local steep bathymetry and depths of thermoclines/haloclines. The optimization parameters were the

Pierre F.J. Lermusiaux (pierrel@mit.edu) is Associate Professor, **Patrick J. Haley Jr.** is Research Scientist, **Wayne G. Leslie** is Research Scientist, **Arpit Agarwal** is PhD Candidate, **Oleg G. Logutov** is Postdoctoral Scientist, and **Lisa J. Burton** is PhD Candidate, all in the Department of Mechanical Engineering, Massachusetts Institute of Technology, Cambridge, MA, USA.

bathymetric slope and reduced slope, and the vertical gradients of temperature/salinity. Simulations were run for each optimized level. The final levels were those that led to better simulations.

Due to the complexity of the region, we found that the V12.1 (2009) of the Smith and Sandwell (1997) topography was not always very accurate, at times too shallow compared to the depth of ocean water measurements or very different from bathymetric ship data. Because topography is a key variable in the region, in the present simulations, we therefore updated the V12.1 (2009) topography with bathymetry extracted from hydrographic profile data (Craig Lee, University of Washington, *pers.*

> **THE PURPOSE OF THE PRESENT STUDY IS TO DESCRIBE AND REVEAL SUCH REGIONAL OCEAN FEATURES AS ESTIMATED BY A MULTIRESOLUTION, TIDALLY DRIVEN OCEAN MODEL FOR THE FEBRUARY AND MARCH 2009 PERIOD, WITHOUT ANY IN SITU DATA ASSIMILATION.**

comm., 2009), ship bathymetry, and hydrographic data (Arnold Gordon and Zachary Tessler, Lamont-Doherty Earth Observatory, *pers. comm*., 2010). Specifically, we replaced the Smith and Sandwell data if the hydrographic data were deeper or if ship bathymetry data were available, solving a local diffusion equation (MSEAS Group, 2010) to merge the data sources and ensure bathymetric continuity.

Initial and Boundary Conditions

Simulations were initialized using NODC World Ocean Atlas 2005 (WOA05) climatological profiles (Antonov et al., 2006; Locarnini et al., 2006). WOA05 profiles for the month of February were used for the 0–1500-m depth range, and winter profiles from 1500 m to the bottom. The profiles were gridded using a new objective analysis scheme (Agarwal and Lermusiaux, 2010), which computes the length of shortest sea paths among model and data points using the Fast Marching Method and then uses these distances in the covariance models.

Because the NODC database does not contain any CTD data in the Sulu Sea for February, the WOA05 climatology estimates this salinity as an unrealistic mixture of surrounding water masses. We corrected for this issue using our new objective analysis and initialization schemes. Specifically, because our goal is to use only historical data, we initialized our re-analysis for February in the Sulu Sea using historical CTD data for March. This method ensures that Sulu Sea water masses are in the Sulu Sea. The same issue occurs for the Bohol Sea, and we

proceeded similarly.

Also used for the initial conditions are SSH anomaly data from the University of Colorado (Leben et al., 2002) and sea surface temperature fields from the Global Ocean Data Assimilation Experiment (GODAE) High Resolution Sea Surface Temperature Pilot Project (GHRSST-PP) provided by the UK National Centre for Ocean Forecasting through the Operational Sea Surface Temperature and Sea Ice Analysis (OSTIA) program. The SSH data were converted to surface pressure by multiplication with ρg. From this pressure field, a surface velocity anomaly was constructed from a weak geostrophic constraint. The magnitudes of these anomalies were limited to 40 cm s^{-1} by a hyperbolic tangent scaling factor applied to speeds greater than 20 cm s^{-1}. The resultant velocities were extended in the vertical using a Gaussian covariance with a 500-m decay scale. The SSH and SSH-derived velocity anomaly fields were then merged with the surface elevation and velocity derived from the gridded WOA05 profiles (MSEAS Group, 2010). All simulations presented next were initialized on February 2, 2009.

For open boundary conditions (OBC), the transports from the HYbrid Coordinate Ocean Model (HYCOM; Bleck, 2002) obtained from the Naval Research Laboratory-Stennis (E. Joseph Metzger, Harley Hurlburt, and colleagues, NRL, *pers. comm*., 2009) were merged with the transports derived from the gridded profiles and satellite SSH anomalies. For surface boundary conditions, in real time (see next section), we employed Coupled Ocean/Atmosphere Mesoscale Prediction

System (COAMPS) fluxes for wind stress (0.2 degree resolution; Hodur, 1997) and the US Navy's Operational Global Atmospheric Prediction System (NOGAPS) fluxes for net heat flux and evaporation-minus-precipitation (1.0 degree resolution; Rosmond, 1992). After IOP-09, we obtained several other atmospheric forcing products. We completed extensive evaluations of these surface fluxes, and for the re-analysis results (see later section on Re-Analysis and Selected Physical Dynamics Results) we selected the COAMPS archive fluxes (27-km/9-km resolution; Hodur, 1997) for wind stress, net heat flux, and evaporation minus precipitation.

For barotropic tidal forcing, we use our multiresolution tidal elevation and velocity estimates (Logutov, 2008; Logutov and Lermusiaux, 2008), which are derived by generalized inversion from global tidal boundary conditions (Egbert et al., 1994; Egbert and Erofeeva, 2002). Our inversion aims to refine the global estimates and resolve local tidal fields using our high-resolution bathymetry, specific barotropic tide dissipations, and additional data. Our tidal fields (see next section) are then added as time-dependent external forcing at the OBCs of our free-surface simulations. The barotropic tidal elevations and velocities are also added to the initial subtidal conditions.

Data for Assimilation and Model Evaluation

SSH anomalies are the only synoptic data assimilated when available, about every four days to a week. No in situ synoptic data are used because one of the PhilEx goals is to evaluate whether only assimilating remotely sensed data in tuned models can capture some dynamics. Our total dependency on sparse remotely sensed satellite data to initialize and maintain the synoptic features is one of the novel aspects of the present study.

Measurement data available for evaluations of model estimates and for data-model comparisons include: 125 CTD stations, underway temperature, and acoustic Doppler current profiler (ADCP) velocities from R/V *Melville* (Tessler et al., 2010; Gordon et al., 2011); ADCP data from moorings (Janet Sprintall, Scripps Institution of Oceanography, *pers. comm.*, 2010); drifters (Ohlmann, 2011); profiles from the Global Temperature and Salinity Profile Project (GTSPP); and profiles from the EN3 data set of the UK Meteorological Office, Hadley Centre (Ingleby and Huddleston, 2007).

In total, for the derivation of new methods and codes for generic archipelago regions and for physical, biogeochemical, and numerical parameter tuning and real-time forecasting, more than 3,000 simulations were so far run in this region for the three expedition periods of 2007, 2008, and 2009. Only a subset of the real-time results and of the re-analysis studies is provided next.

SELECTED REAL-TIME PREDICTION RESULTS

Due to the complexity of the archipelago, very significant modeling system improvements were completed prior, during, and after the three real-time experiments. Of course, various model parameters (e.g., bottom friction, mixing) were tuned, but more importantly, new methods were developed and software built for complex archipelagos with topographic barriers and multiply connected domains. These improvements include new schemes for: (1) objective mapping using Fast Marching Methods (Agarwal, 2009; Agarwal and Lermusiaux, 2010); (2) optimizing the many interisland transports in initializations from geostrophic shear (Agarwal et al., 2010); (3) region-dependent biological initialization; (4) multiscale fully implicit two-way nesting (Haley and Lermusiaux, 2010); and (5) generalized inversion for high-resolution barotropic tidal fields (Logutov and Lermusiaux, 2008). Without these schemes, we could not model the region. During the real-time 2009 exercise (Lermusiaux et al., 2009), forecasts of physical and biological fields were generated at three- to four-day intervals, remotely sensed products (SST, SSC, SSH) were used for evaluation, and descriptive dynamics summaries and adaptive sampling guidance were disseminated. Re-analyses were also completed in real time, for both the physics and the biology, at various resolutions in the different domains. Only SSH data were assimilated every four days to a week.

Coupled Physics-Biology IOP-09 Real-Time Predictions

The Dusenberry-Lermusiaux biological model (Besiktepe et al., 2003) was used. The six state variables were initialized using a new region-dependent procedure, reflecting the many topographic barriers of the archipelago. First, a synoptic chlorophyll three-dimensional initial field was created from satellite SSC data (Robert Arnone, NRL, *pers. comm.*, 2009) and region-dependent generic profiles. Satellite data were combined over a two-week period

(January 24–February 7, 2009) to provide sufficient initialization coverage. The archipelago domain was divided into four regions that are distinct biologically (South China Sea, shallow interior seas, Sulu Sea, and Pacific-Sulawesi Sea). Generic parametric chlorophyll profiles were created for each region based on experimental data from Cordero et al. (2007). Final initial profiles were then created by scaling the parameters of the generic profiles at each location such that their integration over the euphotic zone would match the SSC data. The initial nitrate and ammonium fields were then estimated using WOA climatology and our new objective mapping schemes (Agarwal and Lermusiaux, 2010). The remaining phytoplankton, zooplankton, and detritus initial fields were then dynamically computed using the biogeochemical reaction terms of our equations in a weak constraint form, with parameters estimated from the literature. Specifically, we integrate the reaction terms with a fixed-point iteration scheme (Chapra and Canale, 2009), leading to fields in a quasi-dynamical equilibrium that depend on the equation parameters. Hence, the choice of parameters and of initial conditions is coupled.

After initialization, no biological data were assimilated. Specifically, no SSC was used after February 2, 2009. To evaluate the skill of our real-time biological forecasts, the only biological data available that have some coverage are the weekly SSC composites (Figure 2a–c). Modeled chlorophyll fields were thus integrated into sea surface chlorophyll and averaged over one week. As Figure 2 shows, and as described below, the forecast field patterns and their evolution have some similarities with those of

the SSC data. To evaluate this similarity quantitatively, we compared the skill of the weekly model estimates to the skill of the "persistence of day zero" (i.e., the model initial conditions on February 2, 2009). For the weeks in March shown in Figure 2, the model estimates are closer to the SSC data in the root-mean-square-sense by 1 to 6%. This improvement is minor compared to persistence of the initial conditions, but it shows that forecasts without any data can already be valuable. Further calibration of the model and its initial conditions, but also of the SSC data (which can have unrepresentative values), is necessary for greater skill.

Specific variability patterns to note during February 2009 are the strong and horizontally extended biological activity in the Visayan and Sibuyan seas (Figure 2b,d–f) in response to northeast monsoon wind mixing, and in the shallow Cuyo Island West passage (Figure 2c,d–f) in response to topography-driven subsurface upwelling of deeper, nutrient-rich SSC waters on the shelf west of Mindoro Strait. The model forecasts also captured the blooms in the shallower shelf waters of the western Sulu Sea, in part driven by inflows through Balabac Strait (see Circulation Features in next section) of nutrient-rich waters also from the deeper SSC. Vertical sections (not shown) indicate that part of these shelf blooms are also sustained by internal wave mixing and by turbulent mesoscale gyres and eddies of the Sulu Sea (Figure 3) interacting with the shallow shelf. Biological blooms driven by internal wave and water mass mixing also occur on both sides of the Sulu Archipelago (south of the Sulu Sea from Borneo to Mindanao), as well as

on the northern side of Palawan (see the chlorophyll evolution in both the model and SSC fields in Figure 2, noting that model forecasts underestimate the amplitudes of Sulu Archipelago blooms). However, and interestingly, south of the middle Palawan and Honda bays, chlorophyll is forecast and observed to be depleted (e.g., Figure 2e–f). A lesser but still visible low-chlorophyll pool is also estimated on top of the Iligan Bay Eddy, a property previously observed (Cabrera et al., 2011). Note, however, the coastal-upwelling-driven bloom just southwest of Dipolog Strait (Figure 2e–f), along the Zamboanga Peninsula (Villanoy et al., 2011). A final highlight of these forecasts is a frequently observed feature in northeast monsoon conditions (Dolar et al., 2006; May et al., 2011)—the wind-jet-driven upwelling off Verde Island Passage north of Mindoro and the corresponding biological bloom being advected offshore into "mushroom" patterns of eddies (Rypina et al., 2010). Our estimates indicate that this bloom and its advection pattern develop in two weeks (Figure 2e–f). Of course, these physical-biological forecasts were only a first, albeit promising, attempt to predict biogeochemical features in a very complex, multiregion-equilibrium archipelago, without any in situ data assimilation. Due to couplings, detailed biological dynamics studies would require further improvements in both the physics and the biology, and are beyond the scope of this work.

Inverse High-Resolution Barotropic Tidal Modeling

Tidal forecasts and descriptions were provided to support the observational and modeling work in real time. Data

from ADCP moorings (Janet Sprintall, Scripps Institution of Oceanography, *pers. comm.*, 2010) were used to tune the tidal model and obtain the inverse estimates of the tidal OBCs used to force our ocean model. The largest constituents are M2, S2, K1, and 01, leading to both diurnal and semidiurnal components and interactions.

Tides were found to dominate the dynamics in Surigao and San Bernardino straits, with model and observed velocities up to 150 cm s⁻¹. The spatial structures of the flow fields through these two straits and shallower seas to the west, such as the Sibuyan and Visayan seas, are highly spatially inhomogeneous (not shown), which makes the role of models in predicting the flow fields and de-tiding the measured currents indispensable. Our high-resolution inverse techniques (Logutov, 2008) also proved necessary to capture the often abrupt phase changes of barotropic tidal flow fields through the straits, leading to complex mixing patterns and variability within the straits proper. Considering the straits reaching the Sulu Sea, Balabac Strait to the west and Sibutu Passage to the southwest are also tidally very active, with the Sibutu region known to be a generation site of strong solitons (Apel et al., 1985). We note that such nonlinear
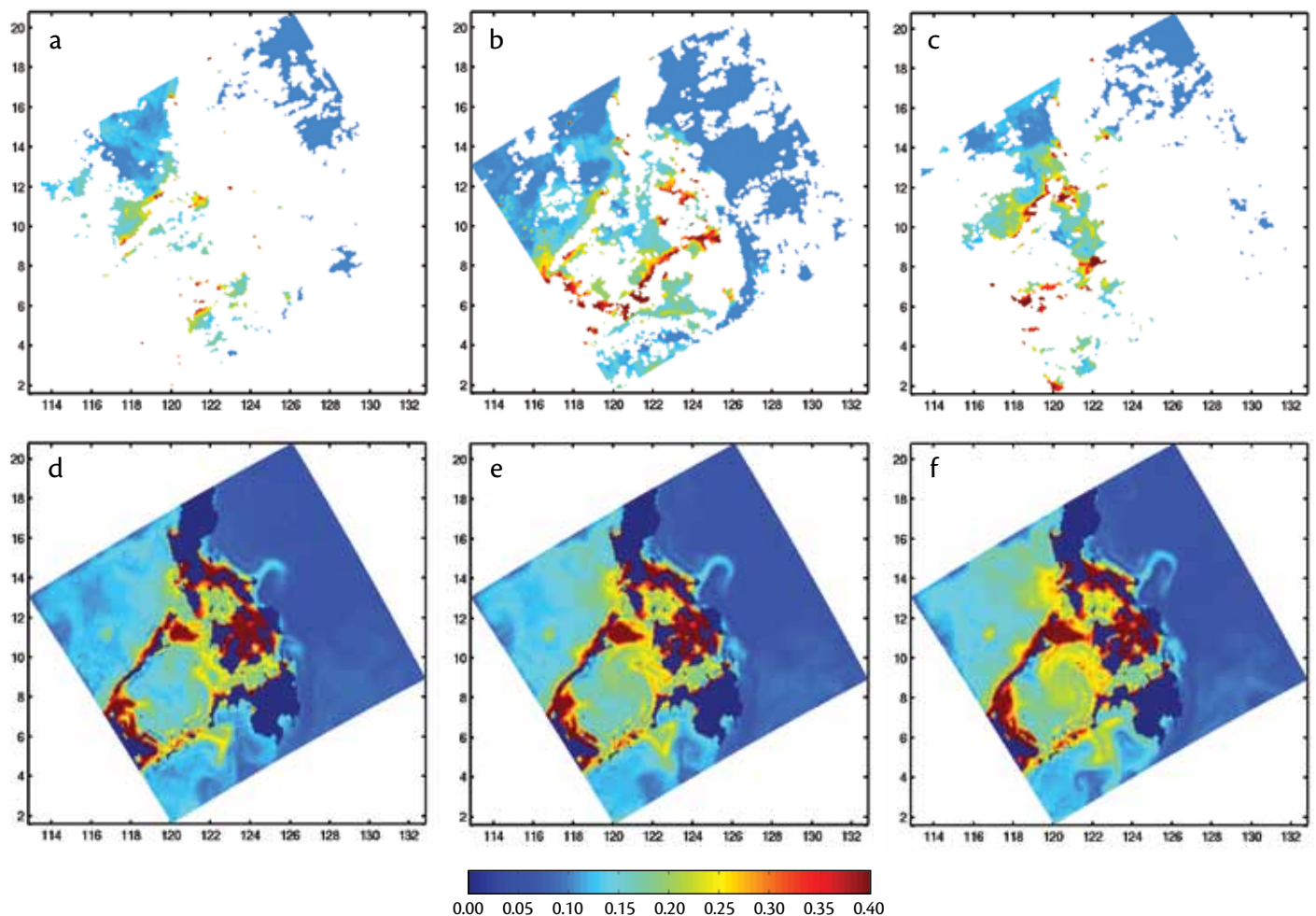

Figure 2. Comparison of MIT Multidisciplinary Simulation, Estimation, and Assimilation System (MSEAS) chlorophyll (mg m⁻³ of N) real-time forecasts with composites of satellite sea surface color (SSC) imagery. The top panels show satellite composites, and the bottom row the corresponding MSEAS forecasts. (a) and (d) February 26–March 4, 2009. (b) and (e) March 5–11, 2009. (c) and (f) March 12–18, 2009. Note that the satellite data are limited due to cloud cover. Modeled chlorophyll forecasts were integrated into sea surface chlorophyll and averaged over one week, so as to allow comparisons with weekly SSC composites. Neither in situ biological nor SSC data are assimilated. All forecasts start from the same initial condition on February 2, 2009; thus, panel (d) is 24 days into the forecast simulation.

waves are not resolved in our simulations: when vertical and horizontal scales become similar, a nonhydrostatic model is needed. Northeast of the Sibutu region, but still within the Sulu Archipelago, there are several other shallower straits such as Basilan Strait and Tapiantana Channel, where tidal effects are also significant. The roles of the Sulu Archipelago straits and shelf-breaks in the formation of deep Sulu Sea water are discussed in the next section.

Circulation Features

Figure 3 provides model estimates of ocean currents and salinity fields averaged over selected depth ranges
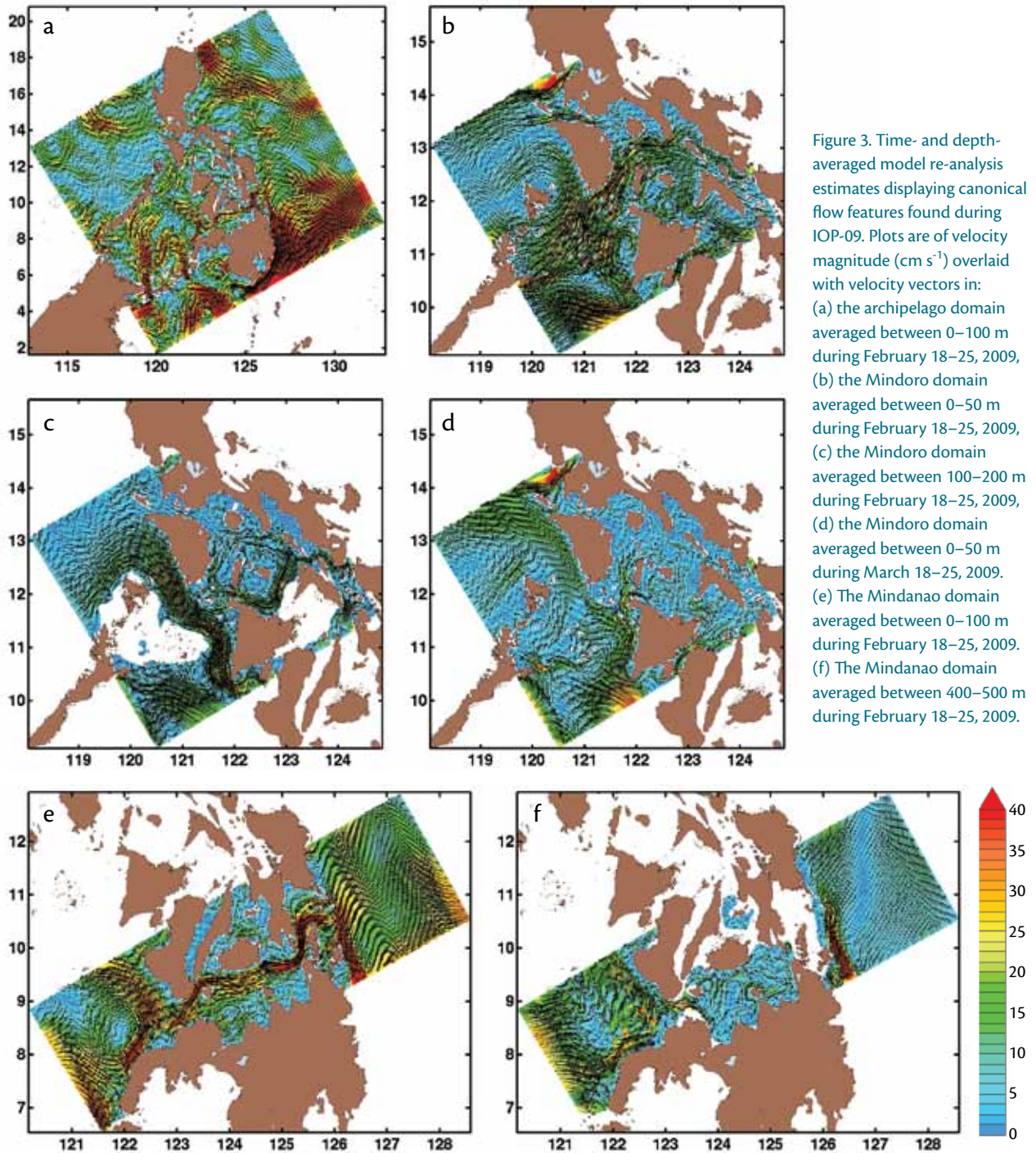

Figure 3. Time- and depth-averaged model re-analysis estimates displaying canonical flow features found during IOP-09. Plots are of velocity magnitude (cm s^{-1}) overlaid with velocity vectors in: (a) the archipelago domain averaged between 0–100 m during February 18–25, 2009, (b) the Mindoro domain averaged between 0–50 m during February 18–25, 2009, (c) the Mindoro domain averaged between 100–200 m during February 18–25, 2009, (d) the Mindoro domain averaged between 0–50 m during March 18–25, 2009. (e) The Mindanao domain averaged between 0–100 m during February 18–25, 2009. (f) The Mindanao domain averaged between 400–500 m during February 18–25, 2009.

and during February 18–25 and March 18–25, 2009. In the following, and in Figure 4, we compare the data collected from R/V *Melville* (see Gordon, 2011) with our model estimates.

From the Pacific Ocean, the North Equatorial Current impinges upon the Philippine Archipelago and splits into two boundary currents (around 14°N; Qu and Lukas 2003): the equatorward Mindanao current and the creation of the northward Kuroshio (Figure 3a). Instead of a laminar stagnation point flow, the separation zone is estimated as a wedge-shaped eddy field separating and joining the two currents. A portion of the Mindanao current flows along the island of Mindanao into the eastern Sulawesi Sea, advecting in the saline Pacific waters between 100–200 m (not shown). North of the Philippines, Pacific waters can enter the South China Sea through Luzon Strait (outside of our archipelago modeling domain). The Mindoro Strait system (Figure 3b–d) connects the South China Sea to the Sulu Sea (through the Panay sill) and to the Sibuyan Sea (through Tablas Strait). Near the surface, the flow in Mindoro and Panay straits starts out southward on average in February (Figure 3b) in response to the northeast monsoon (May et al., 2011), but swings around to a northward average for the last weeks of February and March (Figure 3d), consistent with the March 2009 observations of Gordon et al. (2011) and shown in Figure 4c. At depth, the flow through this strait is predominantly southward (Figure 3c), weaker at mid depth and much stronger near the bottom (Tessler et al., 2010). At the mouth of the Panay sill, in the Sulu Sea, the cyclonic surface Panay eddy is present during mid to late February

(Figure 3b) before being mostly absorbed into northward surface flow (Figure 3d). For most of February and March 2009, the flow in Tablas Strait is weak and variable (into and out of the Sibuyan Sea at different periods; Figure 3d). The South China Sea has two additional connections to the Philippine Archipelago.

> **"...VARIOUS MODEL PARAMETERS (E.G., BOTTOM FRICTION, MIXING) WERE TUNED, BUT MORE IMPORTANTLY, NEW METHODS WERE DEVELOPED AND SOFTWARE BUILT FOR COMPLEX ARCHIPELAGOS WITH TOPOGRAPHIC BARRIERS AND MULTIPLY CONNECTED DOMAINS."**

The first is through Balabac Strait. In February to March of 2009, the mean flow through Balabac Strait is eastward into the Sulu Sea (Figure 3a). The second is through the Verde Island passage directly into the Sibuyan Sea. In our simulations, the weekly mean flow there is variable, changing direction and overall magnitude depending on which week is averaged (not shown). The Sibuyan Sea also has a direct connection to the Pacific Ocean through San Bernardino Strait. Although tidally very active (Jones et al., 2011), the mean flows through the strait are negligible (Figure 3b–d). This estimation agrees with the observations of Gordon et al. (2011) who found no CTD or ADCP evidence of San Bernardino water penetrating far into the Sibuyan or Camotes seas.

Further south, in the Bohol Sea, the time/depth averaged (upper 100 m)

fields show an inflow from the Pacific through Surigao Strait into the Bohol Sea, joining up with the Bohol jet along the northern edge of the Bohol Sea (Figure 3e). This model result is consistent with measurements (Gordon et al., 2011; Hurlburt et al., 2011; see also Figure 4e). The Bohol jet continues

through Dipolog Strait and into the Sulu Sea where it joins a cyclonic eddy and proceeds northward along Negros Island. In the western Bohol, the southern edge of the Bohol jet merges with the cyclonic Iligan Bay Eddy (Figure 3e). In our simulation, during late February, the Iligan Bay Eddy bifurcates at its western edge into the main eddy and a coastal current that follows Iligan Bay proper until it rejoins the main eddy near Sulauan Point. At depth (400–500 m), the flow through Dipolog Strait is eastward from the Sulu Sea into the Bohol Sea (Figure 3f; Gordon et al., 2011). At intermediate depths, the flow through Dipolog Strait is more variable. The Sulu Sea itself has a fairly complex eddy field with a general cyclonic flow. On average, over the two-month period, the Sulu Sea has a net inflow from Balabac, Mindoro/Panay, and Dipolog

straits and net outflow through the Sibutu Passage and the Sulu Archipelago (Figure 3a). Although Sibutu Passage has a net outflow, it is tidally very active and experiences episodic net inflows from the Sulawesi Sea (especially in the bottom layers). The Sibutu tides generate strong internal tides and internal waves (Apel et al., 1985; Girton et al., 2011; Jackson et al., 2011) but we also find strong internal tides and waves along the southern rim of the Sulu Sea by the western half of the Sulu Archipelago steep shelfbreak. Smaller but appreciable internal tides/waves also occur along the western edge of the Sulu Sea from Borneo across Balabac Strait to Palawan Island. These sites provide a
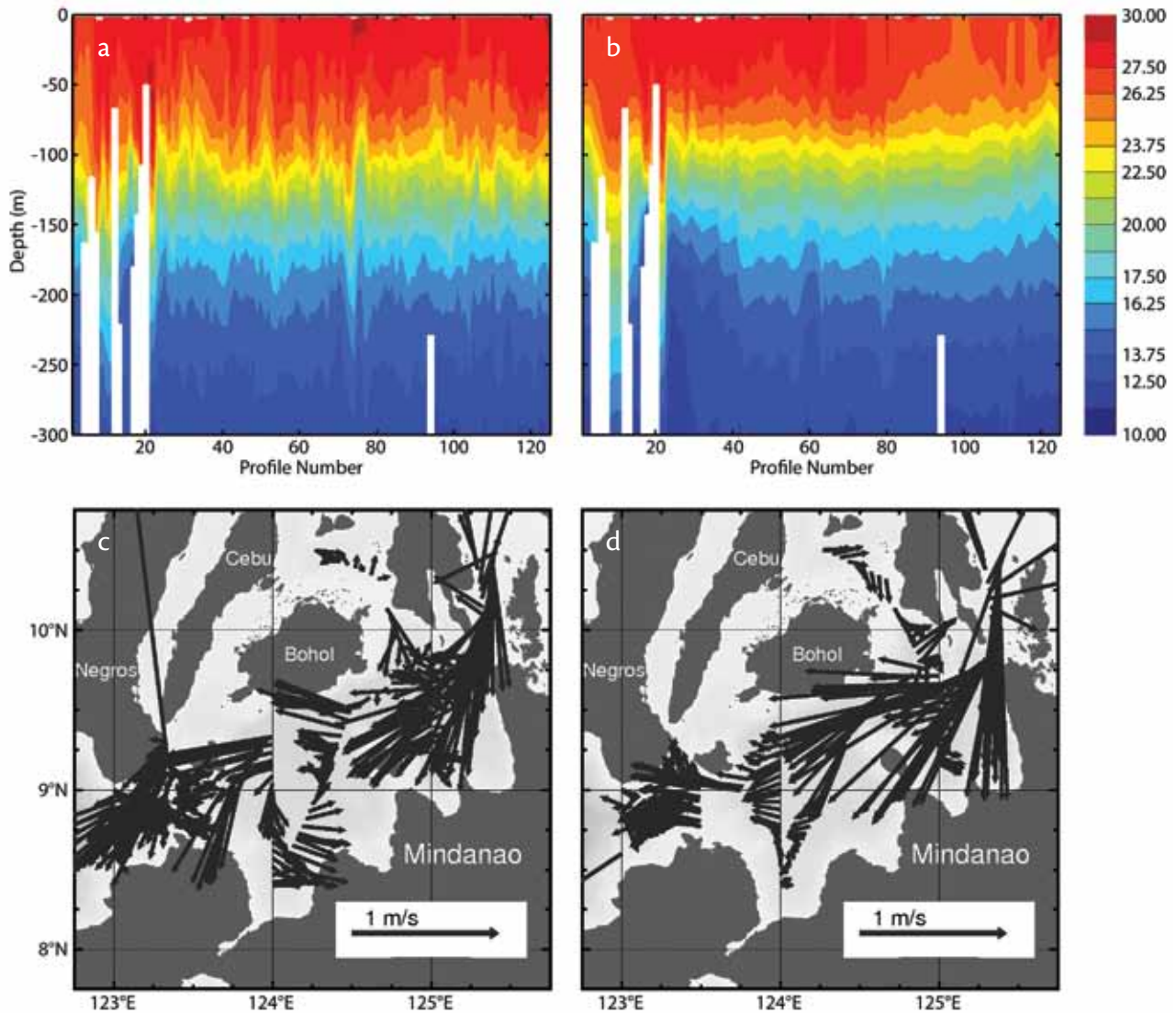

Figure 4. Comparisons of in situ data and model re-analysis results. (a) *Melville* CTD casts and (b) model temperature (°C) estimates. *Melville* profiles 1–22 were collected within the San Bernardino region, out to the Pacific and back through shallower seas and island chains towards the Bohol Sea over the period February 28–March 3, 2009. Profiles 23–40 were collected from March 3–5, 2009, within the Bohol Sea. Profiles 41–63 were collected in Dipolog (Mindanao) Strait and westward into the Sulu Sea over the period March 5–9, 2009. The Sulu Sea to the coast of Panay was covered by stations 64–85 from March 9–15, 2009. From March 15–17, *Melville* was off Panay, went into Tablas Strait, and returned to the Panay sill region. Mindoro Strait was sampled from March 17–20. (c) Velocity vectors (see scale of 1 m s⁻¹) of underway ADCP data averaged over the depth range 23–55 m during March 3–5. (d) Corresponding model velocity vectors. Model estimates generally reproduce the structures found in the underway ADCP data, but are weaker than observations in the Mindoro region (not shown), in part due to the non-use of in situ data and to errors in the SSH data and atmospheric forcing.

mixing mechanism for the generation of Sulu deep water.

To compare our model estimates to data, we show the temperature measurements from 125 CTD stations (Figure 4a) and the ship-underway ADCP velocities averaged from 23–55-m depth in the Mindanao regions (Figure 4c). Figure 4b and d, respectively, give the corresponding model estimates. The evolution of the temperature profile and the main thermocline along the ship tracks (Figure 4a) is relatively well captured by our simulations (Figure 4b), except for the atmospheric-driven surface cooling and upwelling at the end of the track in the Mindoro region, which is too strong (simulations without atmospheric forcing maintain the surface temperature structure). The simulations also exhibit some faster internal tide and wave effects: a strong one just before profile 80 is almost at the right time, even though the model resolution is still too coarse to capture all the finer observed scales. The surface velocities simulated in the Mindoro region (not shown) are overall in the right directions, showing northward flow within Mindoro Strait into the South China Sea, the Panay eddy and several features of the Sibuyan Sea. However, model currents are a bit too weak there, likely due to the larger-scale forcing by remotely sensed SSH, which is often erroneous in shallower regions, and to the lack of fine-scale in situ hydrographic features in the initial conditions (no in situ data are used). In the Bohol Sea, model estimates (Figure 4d) are in close agreement with observations, showing all features, with the exception of parts of the return flow of the Iligan Bay Eddy, which is weaker in the model during that period, even though it is simulated at most other times (Figure 3e). This issue is again due to the assimilation of SSH data, which we found erroneous during that period.

Flows Within Straits and Transports to the Sulu Sea

Figure 5 compares the time series of measured and simulated along-strait velocities at the Panay, Mindoro, and Dipolog moorings (Janet Sprintall, Scripps Institution of Oceanography,
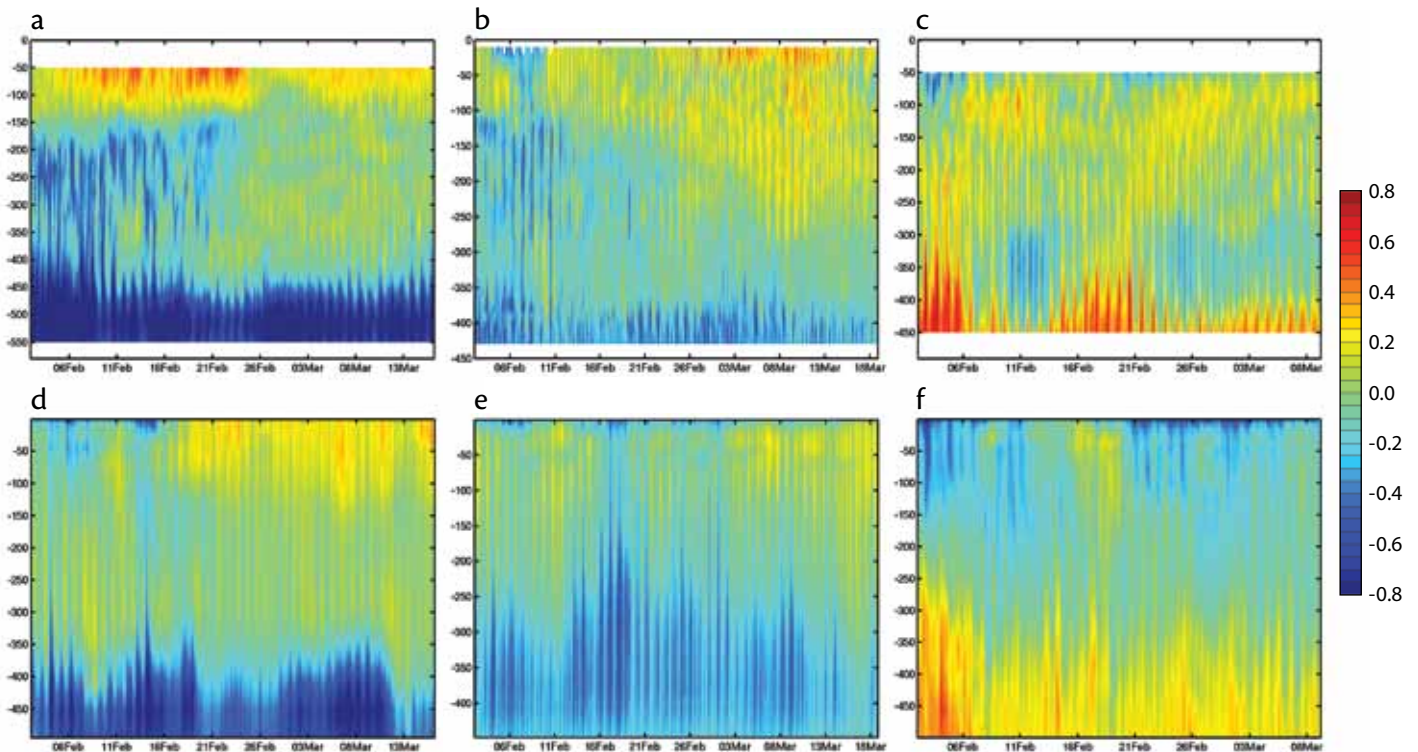

Figure 5. Comparison of observed and modeled along-strait velocity (m s⁻¹) over the period from February 2, 2009, until the recovery of each individual mooring (for all straits, negative values indicate flow into the Sulu Sea). The top row shows observations at moorings: (a) Panay, (b) Mindoro, and (c) Dipolog. The bottom row shows model re-analysis estimates: (d) Panay, (e) Mindoro, and (f) Dipolog. The model estimates are in generally good agreement with the features of the observed flows, for example, the bottom-intensified flows especially at Panay and Dipolog, even though no synoptic in situ data are used in the re-analysis.

pers. comm., 2010). Our simulated flows through the straits proper are in generally good agreement with the strength, direction, and structure of the observed flows, for example, the bottom-intensified flows at Panay and Dipolog. This result is significant because many factors could lead to large differences, including: (1) no synoptic in situ data are used, not even in the initial conditions; (2) the local bathymetry is very tortuous, uncertain, and only simulated at 3-km resolution; and (3) the assimilation of SSH every four days to one week does not resolve strait flows. The first common property is that tidal effects are clearly significant. At Panay (Figure 5a,d), the simulated along-strait bottom flow is negative, to the Sulu

Sea, but is a bit underestimated due to the limited bathymetric resolution and lack of synoptic data. The mid-surface flow is weak, tidally modulated, and on average southward to the Sulu Sea, but starts to reverse by the second week of March. The surface flow is northward to the South China Sea as observed, except at the start of the simulation, likely due to too large COAMPS wind forcing. At Mindoro (Figure 5b,e), as observed, the surface and mid-depth flows are weak and southward, progressively reversing with time and depth. The surface flow reverses northward toward the South China Sea in late February, while the mid-depth flow becomes a weak northward flow by the first weeks of March. At the bottom, the flow remains to the

south into the Sulu Sea, but it is, again, a bit too weak in the simulations, largely due to the 3-km-resolution bathymetry. At Dipolog (Figure 5c,f), the surface (negative) along-strait flow is correctly to the Sulu Sea within the Bohol jet, and the bottom-intensified overflow is from the Sulu Sea to the Bohol Sea. At mid depths, the flow is more variable, with 14-day-period events indicating a progressive mid-depth to mid-surface intensification of inflows to the Bohol Sea, superposed onto mid-depth outflows to the Sulu Sea. All of these simulated properties agree with the synthesis of Gordon et al. (2011).

Figure 6 compares the time-averaged values of the Figure 5 velocity profiles for both the along-strait and across-strait
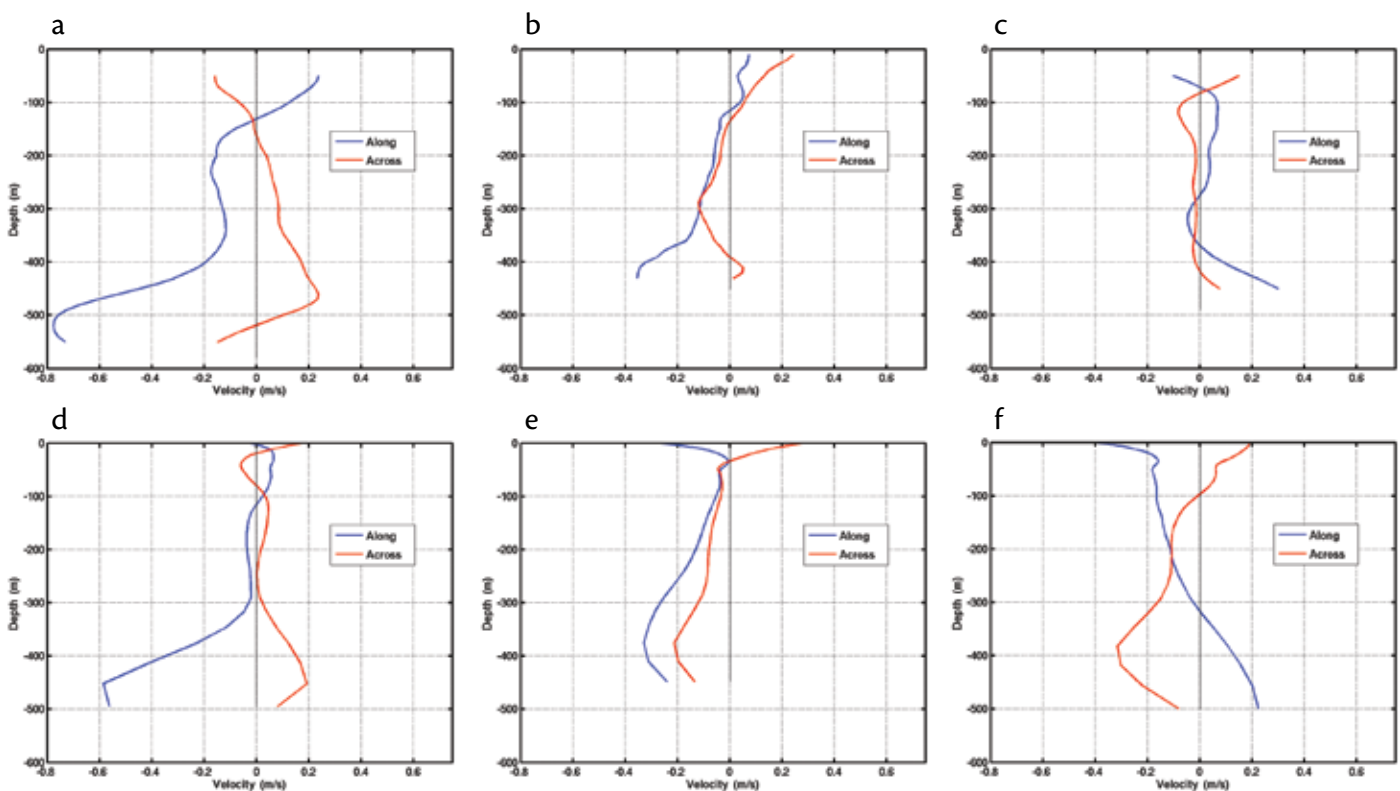

Figure 6. Comparison of time-averaged along-strait (blue) and across-strait (red) velocities (m s⁻¹) over the period from February 2, 2009, until the recovery of each individual mooring. The top row shows observations at moorings: (a) Panay, (b) Mindoro, and (c) Dipolog. The bottom row shows model re-analysis estimates: (d) Panay, (e) Mindoro, and (f) Dipolog. Even though no in situ data are assimilated, the structures of the simulated mean profiles agree overall with those of the observed means.

directions. The mean profiles confirm all of the along-strait findings shown in Figure 5, this time for time averages. It is surprising, perhaps, that even the across-strait mean flows are relatively well captured, even though the nested-domain resolution is still a bit too coarse for these smaller-scale processes that are in part controlled by each strait's width, which can be very short at depth. The shape of the across-strait flow is off only for the deep Dipolog Strait, due to the sharp meanders of the real Dipolog at depth, which are not represented in the 3-km-resolution bathymetry.

The above comparisons were made using single mooring positions located at the expected sills of each strait so as to sample the deepest overflows. To extend these results, we now examine the overall water transports across sea segments between islands, focusing on the Sulu Sea during IOP-09. To accurately estimate these transports into and out of the Sulu Sea, we employ an algorithm consistent with the conservation of mass imposed by our nonlinear free surface model (see equation 65 in Haley and Lermusiaux, 2010). Specifically, the transport along a line segment is the integral of the terms in the divergence operator along model grid edges that best approximate the given line segment. To find that set of grid edges, we employ the Bresenham (1965) line algorithm. The resulting transports are plotted as functions of time in Figure 7b–f (positive outward), for each of the five open-sea segments surrounding the Sulu Sea (Figure 7a). Through the segment spanning the Sulu Archipelago (Figure 7b), we find a time-average mean 3.68 Sv outflow to the Sulawesi Sea (half of which flows through Sibutu Passage), with a large tidal signal that gives rise to a standard deviation in time of 7.5 Sv. The interplay of diurnal and semi-diurnal tides produces a beat pattern envelope on the tidal signal, leading to several periods of intense instantaneous inflow across the archipelago from the
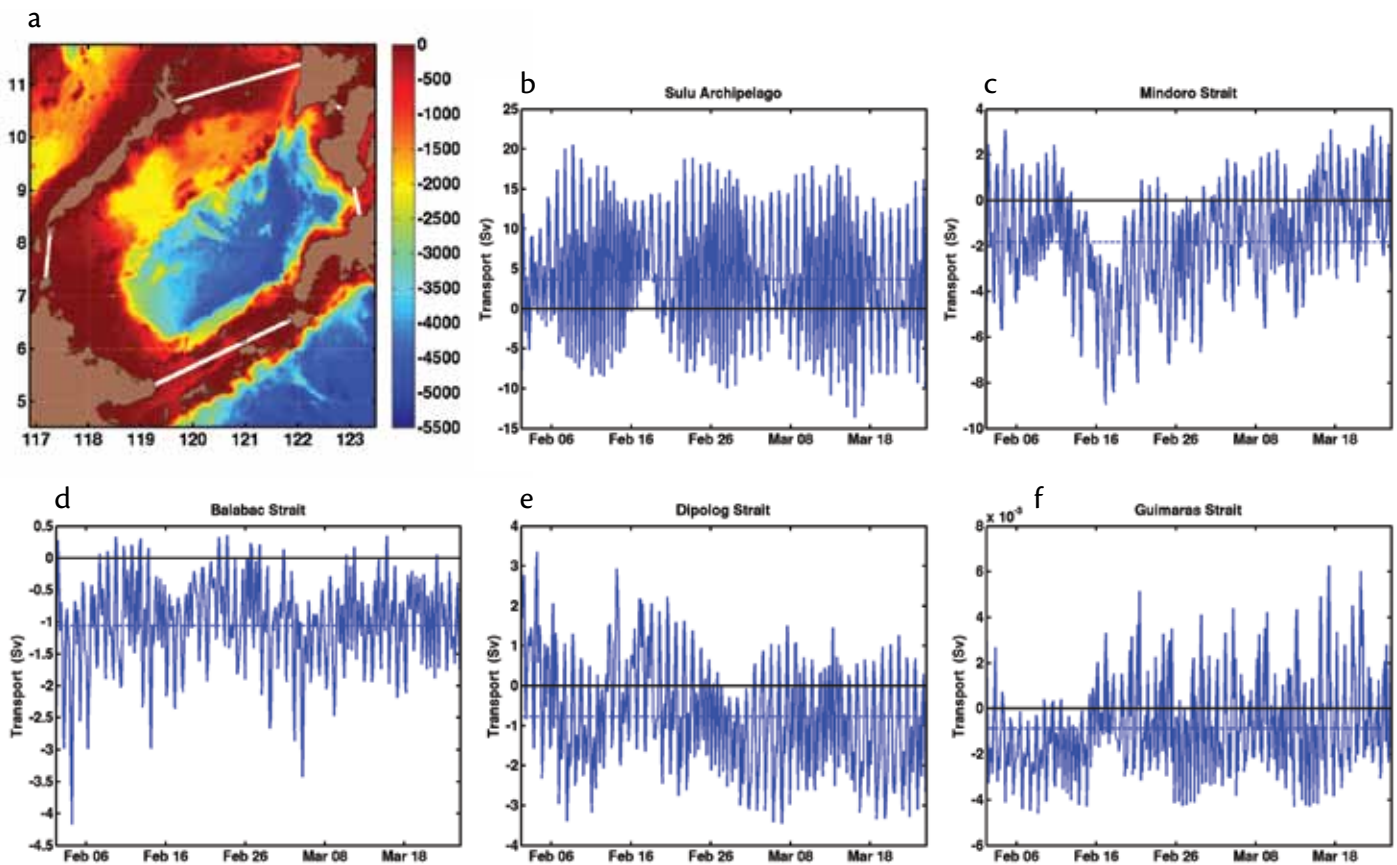

Figure 7. Transports into and out of the Sulu Sea (positive transports are out of the Sulu sea, for an outward normal) during February to March 2009. The figure shows (a) locations of the sections (the five white lines) through which transports are evaluated, and then transports as a function of time through (b) the Sulu Archipelago (+3.68 Sv time average), (c) Mindoro Strait (-1.83 Sv time average), (d) Balabac Strait (-1.06 Sv time average), (e) Dipolog Strait (-0.77 Sv time average), and (f) Guimaras Strait (-9 x 10^{-4} Sv time average).

Sulawesi Sea. The remaining sections, on average, contribute to a mean inflow into the Sulu Sea. Mindoro Strait (Figure 7c, spanning Palawan to Panay) provides a mean 1.83 Sv inflow with a mostly tidally driven standard deviation of 2.4 Sv. The mean is consistent with the observation of Janet Sprintall (Scripps Institution of Oceanography, *pers. comm.*, 2010), who reports a 1–2 Sv southward averaged transport in Panay Strait during the IOP-09 period (the northeast monsoon driving stronger

rise in the Sulu SSH over a time step of 150 sec. Of course, all of these transports and temporal variability are uncertain. Based on the ensemble of simulations that we ran (ensemble members have slightly different numerical schemes, model parameters, initial conditions, and/or bathymetry), the mean transport uncertainties are about 50%. These transport numbers also depend on the open boundary inflows from the Pacific, which would further increase uncertainties (e.g., Arango et al., 2011).

processes likely responsible for this deep-water formation.

The two deepest straits leading to the Sulu Sea are the Panay sill to the northeast (sill depth of ~ 570 m) and Sibutu Passage to the southwest (sill depth near Pearl Bank is ~ 370 m). Figure 8a shows their locations and Figure 8b,d shows the corresponding deep transports as a function of time. Studying the Panay sill first, our results show a net time-average deep inflow of 0.68 Sv to the Sulu (Figure 8b), with a 50% uncertainty standard deviation, and a 0.2 Sv tidal modulation. The mean transport is about twice as large as that obtained by Tessler et al. (2010), which is within our uncertainties. They used the mooring data for the same February to March 2009 time frame and extended the point profile in space using triangular shapes to obtain bottom transport. Several reasons can explain the difference. First, slight changes in that shape or in its extension alter the final estimate. Second, the mooring is at the sill proper and does not sample the whole flow. In fact, the time-averaged velocity section (Figure 8c) reveals an intensified current to the western side of the sill. This observation agrees with a southward density-driven flow along the Mindoro-Panay Strait system and momentum advection in approximate balance with the Coriolis force and bottom stress, with the former deflecting the flow to the right. This finding of western-side intensified flow agrees with hydrographic data (Tessler et al., 2010). Finally, it is worth noting that if we restrict our bottom transport to salinities within 34.43 to 34.46 (not shown), we would divide our transport by more than two. Focusing now on the segment in Sibutu Passage, our simulation shows

> ...THE TIME-AVERAGED VELOCITY SECTION (FIGURE 8C) REVEALS AN INTENSIFIED CURRENT TO THE WESTERN SIDE OF THE SILL...THIS FINDING OF WESTERN-SIDE INTENSIFIED FLOW AGREES WITH HYDROGRAPHIC DATA.

than normal mid-depth southward flow in this strait). Balabac Strait (Figure 7d) provides a mean 1.06 Sv with a mostly tidal 0.7 Sv standard deviation in time, and Dipolog Strait (Figure 7e) a mean 0.77 Sv with a 1.4 Sv standard deviation. In Guimaras Strait (between Panay and Negros; Figure 7f), there is essentially no net flow (9×10^{-4} Sv mean inflow with 0.002 Sv standard deviation). Summing the inflows of these four sections provides a mean 3.66 Sv inflow. The difference between this mean inflow and the above mean outflow is a net 0.02 Sv inflow. This number is exactly equal to the free-surface term in our model equations and is equivalent to a mean 6 mm

Deep Sulu Sea Water

The Sulu Sea is a semi-enclosed basin filled and renewed by waters overflowing the above-mentioned straits and open-sea segments. Its deep water has received recent attention in part because of decadal and climate studies (e.g., Quadfasel et al., 1990; Rosenthal et al., 2003; Gamo et al., 2007; Arnold Gordon and colleagues, *pers. comm.*, 2010). Below 1250-m depth, salinity is slightly stratified, from a minimum of 34.45 to the deep salinity of 34.744, while the temperature is relatively uniform, suggesting that the deep water is a mixture of water masses. We now examine the multiscale

a deep flow (Figure 8d) with strong tidal velocities, but a small net time-averaged inflow of 0.03 Sv into the Sulu Sea from February to March 2009. However, the simulation also shows periods of intense instantaneous deep inflow from the Sulawesi Sea, modulated by spring and neap tides, with twice-a-month to monthly frequencies. This finding is confirmed by the salinity simulated at the strait section (Figure 8a), spatially averaged within 20 m of the bottom (Figure 8e); the deep mean salinity at the section is indeed driven by such slower frequencies, increasing to 34.54–34.56 in periods of inflow from the Sulawesi Sea.

To confirm that these two straits are two main sources for the deep, salty Sulu Sea water, we first focus on the overflows from deep depths. Figure 9a shows the salinity integrated vertically at each model grid point from 200-m to 1000-m depth, but only if the salinities are within 34.45 to 34.55 (salinities outside that range are not considered), and averaged over February 4–11, 2009. Figure 9b shows the corresponding integrated and averaged horizontal velocity. Advection of higher-salinity waters from the subsurface Pacific to the Sulawesi Sea by the Mindanao current is clearly visible, and these waters can ultimately reach Sibutu Passage. The figure also shows the smaller but still sufficiently high salinities of South China Sea waters, which flow in the Mindoro-Panay strait system. Quantitatively, for these two overflows the Panay sill provides averaged salinities around 34.47–34.53, while Sibutu Passage provides averaged salinities around 34.5–34.55, with mixing occurring within each strait. The tidally active Balabac Strait (sill depth ~ 100 m) could at times be a salinity source but our present simulations did not show
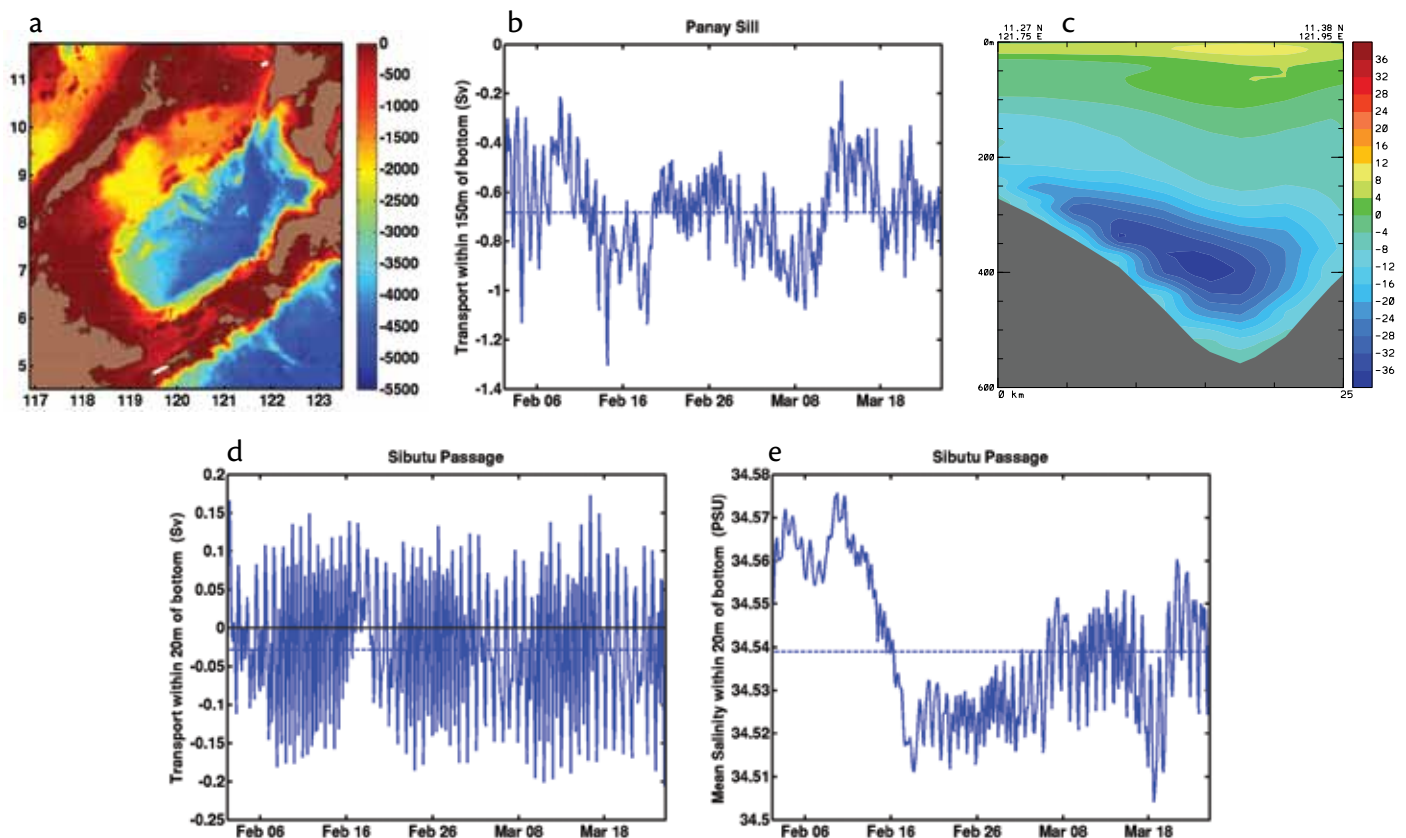

Figure 8. Bottom water transports (Sv) over the Panay sill and through Sibutu Passage during February to March 2009. Positive transports are out of the Sulu Sea (outward normal). (a) Locations of sections (the two white lines) for the Panay sill proper and Sibutu Passage. (b) Transport versus time over the Panay sill within 150 m of the bottom, providing a net time-average inflow of 0.68 Sv into the Sulu Sea, with a 50% uncertainty standard deviation. (c) Velocity (cm s^{-1}, positive into the page), averaged over time during February to March 2009, over the Panay sill, showing the westward deflection of the southern density-driven flow by the Coriolis force. (d) Transport versus time in Sibutu Passage within 20 m of the bottom, showing a small net time-average inflow of 0.03 Sv into the Sulu Sea. (e) Deep salinity (PSU) versus time-averaged salinity along the section (see Figure 9a) in Sibutu Passage within 20 m of the bottom (on time average, the mean salinity is 34.54 PSU).
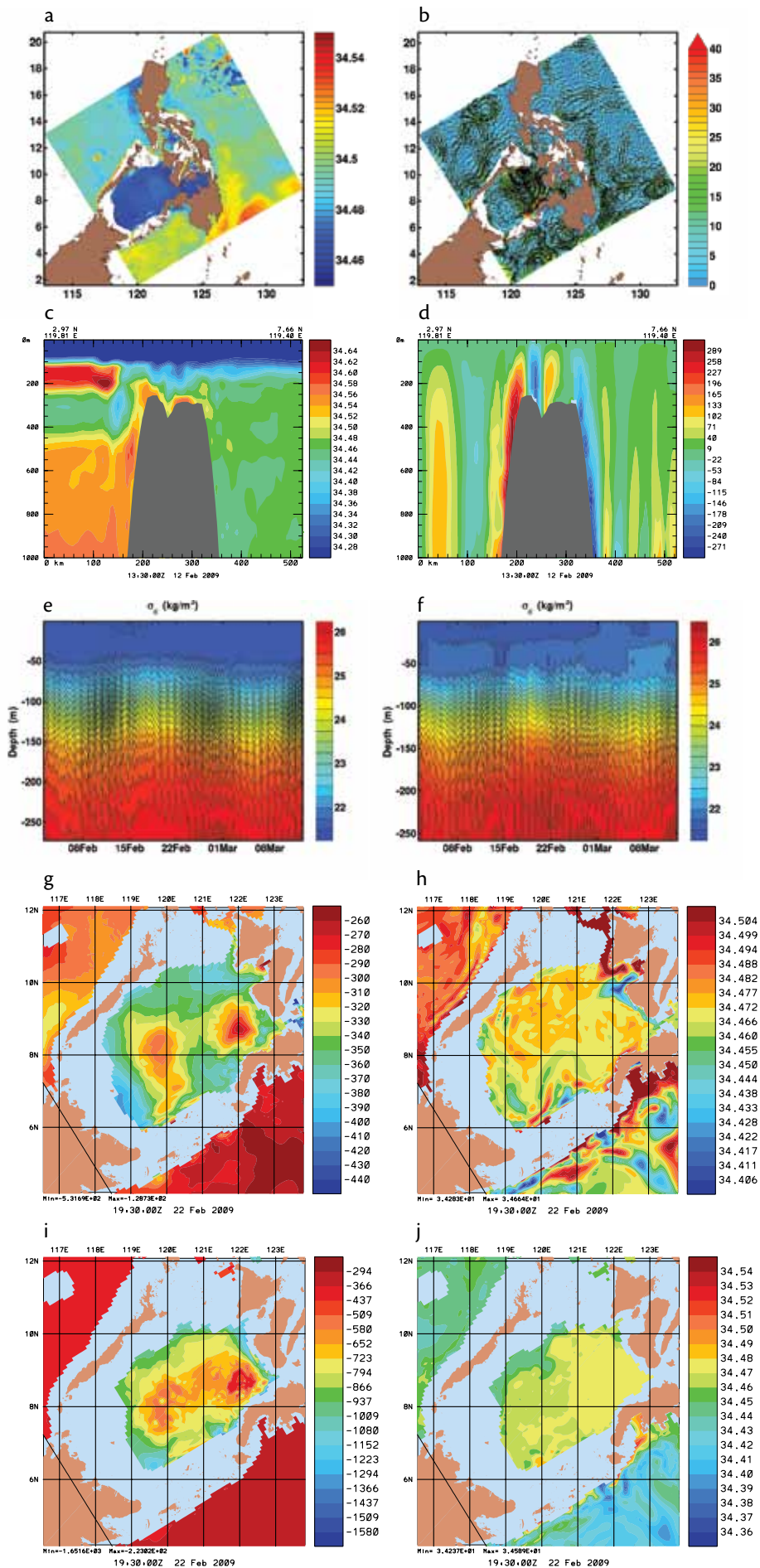
significant inflow events. Finally, strong internal tide/wave signals are visible in the Sulu Sea just north of Sibutu Passage and the Sulu Archipelago (Figure 9a), suggesting a mechanism for deep mixing. This mixing is required because the highest mean salinities in the Sulu Sea are below 1000 m.

Figure 9c,d illustrates the mixing and upwelling/downwelling patterns at Sibutu Passage. Considering the case of pure mixing first, two water masses collide in the upper layers and can be tidally mixed within the 100- to 200-m layer at Sibutu's sills—the subsurface-modified salty Pacific waters are advected in from the Sulawesi and the subsurface waters of the Sulu Sea (less salty at those depths in part due to inflow of more-modified Pacific waters from the South China Sea). In the case of upwelling, Figure 9c,d reveals that deep waters below 700 m can upwell to 200 m, mix within the complex sills and subbasins of Sibutu Passage, and finally

Figure 9. (a) Simulated salinity vertically averaged from 200-m to 1000-m depths, but only if the salinity is within 34.45–34.55 (salinities outside that range are not considered), and temporally averaged over February 4–11, 2009. (b) Corresponding vertically integrated and temporally averaged horizontal velocity (cm s^{-1}). (c) and (d) Salinity and vertical velocity (m day^{-1}) snapshots, in a section along Sibutu Passage from the Sulawesi to the Sulu Sea, as estimated for 13:30Z, February 12, 2009. (e) and (f) Potential density anomalies σ_θ (kg/m^3) as a function of time during February 2–March 13, 2009, at the northern edge of Sibutu Passage (5.8°N, 119.5°E) and at the steep northern shelfbreak of the Sulu Archipelago (6.2°N, 120.3°E), respectively. (g) and (h) Depth of the surface of the constant potential density anomaly σ_θ = 26.15 and the salinity on this surface, respectively, both estimated for 19:30Z on February 22, 2009. (i) and (j) As (g) and (h), but for the density anomaly σ_θ = 26.50.

flow into the Sulu Sea. Our simulations also reveal that these waters can then either downwell and further mix along the steep Sulu Sea bathymetry or advect on the narrow shelves of the Sulu Archipelago. Of course, the vertical velocity patterns (Figure 9d) oscillate with tides (of different phases on each side of the strait) and are not permanent. However, the neap and spring cycles lead to periods favorable to mean upwelling from the deep Sulawesi Sea (see Figure 8e). We find that mixing occurs within tidally driven internal waves both at the entrance and at the exit of Sibutu Passage (subtidal trapped waves are also simulated there), but, in addition, we discover strong internal tides and waves all along the steep shelfbreak on the northern side of the Sulu Archipelago (Figure 9e,f). Several of these waves would develop into deep solitons in the real ocean (nonlinear waves are not resolved by our hydrostatic model; high-resolution nonhydrostatic models would be needed, for example, Ueckermann, 2009; Vitousek and Fringer, 2010). We note that the waves at the northern Sibutu and at the Sulu Archipelago shelfbreak are not in phase, but that stronger tidal events occur every 14 days or so at both locations. These events lead to vigorous mixing of the high-salinity waters (not shown).

To illustrate circulation and mixing in the Sulu Sea, we show the depth of the surfaces of constant potential density anomalies $\sigma_\theta = 26.15$ and $\sigma_\theta = 26.50$ (Figure 9g,i), and the salinity fields on these two surfaces (Figure 9h,j), all estimated on February 22, 2009, at 19:30Z. The inflow from the Mindoro-Panay strait system is clearly visible (Figure 9h). At Sibutu Passage, but even

more so along the Sulu Archipelago, several internal wave trains develop (compare with the first week of February in Figure 9a). As the saltier waters are mixed downward, they form a tongue of higher salinity on which other, deeper internal waves can ride, further increasing the mixing. Note that these deeper internal waves travel at an angle from the Sulu Archipelago (e.g., Figure 9h). The salinity tongue also creates horizontal density gradients that displace the overall cyclonic circulation further offshore, ultimately creating anticyclones on both sides of the tongue (not shown). The depth of $\sigma_\theta = 26.50$ (Figure 9i) reveals a main driver for this tendency toward cyclonic circulation in the Sulu Sea: the sinking, mixing, and advection of heavier salty waters along all of its slopes. The highest salinities on $\sigma_\theta = 26.50$ (Figure 9j) confirm the advection from the Sibutu Passage. However, salinities on heavier σ_θ (not shown) indicate that the strongest mixing and sinking occur at the steep shelfbreak in the middle of the Sulu Archipelago.

CONCLUSIONS

The Philippine Archipelago region is striking for the complexity of its geometry, with multiple islands and passages, and for its multiscale dynamics, ranging from the North Equatorial Current and open-ocean eddies in the Pacific to the very strong tides in shallow areas and the internal waves at steep shelfbreaks. This complexity required novel modeling schemes, including our multiscale objective analyses for such regions (Agarwal and Lermusiaux, 2010), new time-dependent spatial discretizations, and fully implicit two-way nesting in telescoping domains (Haley and

Lermusiaux, 2010). Without these schemes, such multiscale simulations would not have been possible. In the present study, the modeling focus was on the utilization of tuned models using no in situ synoptic data, but only infrequent and sparse remotely sensed sea surface height data.

As described in this special issue, not much was known quantitatively about the region prior to the PhilEx program and its three sea-going expeditions. The scientific simulations described here focused on the IOP-09 period during February to March 2009, and our modeling work aimed to quantify and discover oceanic features in the region. The real-time prediction results presented include a summary of multiresolution tidal properties and a description of the evolution of biogeochemical features focusing on their physical drivers. We also characterized the main circulation features in the whole archipelago region and its many seas, on multiple scales. We estimated and described the evolution and variability of currents within major straits, and we compared these estimates to data collected above the deepest point of three straits. We quantified the transports to and from the Sulu Sea and the corresponding overall water mass balance. And finally, we explored the multiscale mechanisms involved in Sulu Sea deepwater formation.

Opportunities for future multiscale dynamical and process studies are plentiful, including physical and biological-physical dynamics in each strait (e.g., San Bernardino, Surigao, Mindoro, Dipolog, Sibutu, Balabac) and in specific circulation features such as the Iligan Bay Eddy; dynamics of Sulu

Sea gyres and their relationships with overflows and mixing; detailed multi-scale dynamics involved in Sulu Sea deepwater formation; relative contributions of wind-driven vs. density-driven vs. tidally driven circulations, from the shallow to the deep seas; and impacts of larger-scale transports at open domain boundaries. An ultimate goal would be to connect our results to basin-scale and climate studies.

REFERENCES
Agarwal, A. 2009. Statistical field estimation and scale estimation for complex coastal regions and archipelagos. Master's thesis, Massachusetts Institute of Technology, Cambridge, MA.

Agarwal, A., and P.F.J. Lermusiaux. 2010. Statistical field estimation for complex coastal regions and archipelagos. Reports in Ocean Science and Engineering 7, Department of Mechanical Engineering, MIT, Cambridge, Massachusetts.

Antonov, J.I., R.A. Locarnini, T.P. Boyer, A.V. Mishonov, and H.E. Garcia. 2006. *World Ocean Atlas 2005. Volume 2: Salinity*. S. Levitus, ed., NOAA Atlas NESDIS 62, US Government Printing Office, Washington, DC, 182 pp.

Apel, J.R., J.R. Holbrook, J. Tsai, and A.K. Liu. 1985. The Sulu Sea internal solitons experiment. *Journal of Physical Oceanography* 15(12):1,625–1,651.

Arango, H.G., J.C. Levin, E.N. Curchitser, B. Zhang, A.M. Moore, W. Han, A.L. Gordon, C.M. Lee, and J.B. Girton. 2011. Development of a hindcast/forecast model for the Philippine Archipelago. *Oceanography* 24(1):58–69.

Besiktepe, S.T., P.F.J. Lermusiaux, and A.R. Robinson. 2003. Coupled physical and biochemical data driven simulations of Massachusetts Bay in late summer: Real-time and post-cruise data assimilation. In special issue on "The use of data assimilation in coupled hydrodynamic, ecological and bio-geo-chemical models of the oceans," M. Gregoire, P. Brasseur, and P.F.J. Lermusiaux, eds. *Journal of Marine Systems* 40:171–212.

Bleck, R. 2002. An oceanic general circulation model framed in hybrid isopycnic-Cartesian coordinates. *Ocean Modelling* 37:55–88.

Bresenham, J.E. 1965. Algorithm for computer control of a digital plotter. *IBM Systems Journal* 4(1):25–30.

Broecker, W., W. Patzert, R. Toggweiler, and M. Stuiver. 1986. Hydrography, chemistry, and radioisotopes in the Southeast Asian Basins. *Journal of Geophysical Research* 91:14,345–14,354.

Cabrera, O.C., C.L. Villanoy, L.T. David, and A.L. Gordon. 2011. Barrier layer control of entrainment and upwelling in the Bohol Sea, Philippines. *Oceanography* 24(1):130–141.

Chapra, S.C., and R.P. Canale. 2009. *Numerical Methods for Engineers,* 6th ed. McGraw-Hill Higher Education, Boston, MA, 960 pp.

Cordero, K., C.L. Villanoy, L.T. David, and K. Silvano, 2007. Estimating integrated phytoplankton biomass in the seas around the Philippines. *Proceedings of the 13th Workshop of OMISAR* [Ocean Models and Information System for the APEC (Asia-Pacific Economic Cooperation) Region] *(WOM-13) on Validation and Application of Satellite Data for Marine Resources Conservation*. October 5–9, 2004, Bali, Indonesia.

Dolar, M.L., W.L. Perrin, B.L. Taylor, G.L. Kooyman, and M.N.R. Alava. 2006. Abundance and distributional ecology of cetaceans in the central Philippines. *Journal of Cetacean Research and Management* 8:93–111.

Egbert, G.D., and S.Y. Erofeeva. 2002. Efficient inverse modeling of barotropic ocean tides. *Journal of Atmospheric and Oceanic Technology* 19(2):183–204.

Egbert, G.D., A.F. Bennett, and M.G.G. Foreman. 1994. Topex/Poseidon tides estimated using a global inverse model. *Journal of Geophysical Research* 99:24,821–24,852.

Gamo, T., Y. Kato, H. Hasumoto, H. Kakiuchi, N. Momoshima, N. Takahata, and Y. Sano. 2007. Geochemical implications for the mechanism of deep convection in a semi-closed tropical marginal basin: Sulu Sea. *Deep-Sea Research Part II* 54(1–2):4–13, doi:10.1016/j.dsr2.2006.06.004.

Gangopadhyay, A., A.R. Robinson, P.J. Haley, W.J. Leslie, C.J. Lozano, J.J. Bisagni, and Z. Yu. 2003. Feature Oriented Regional Modeling and Simulation (FORMS) in the Gulf of Maine and Georges Bank. *Continental Shelf Research* 23(3–4):317–353.

Gordon, A.L. 2009. *Regional Cruise Intensive Observational Period 2009*. Technical report, Lamont-Doherty Earth Observatory, Palisades, NY. Available online at: http://www.ldeo.columbia.edu/~agordon/Reports/RIOP09_LEG2_rept.pdf (accessed January 25, 2011).

Gordon, A.L., J. Sprintall, and A. Ffield. 2011. Regional oceanography of the Philippine Archipelago. *Oceanography* 24(1):14–27.

Girton, J.B., B.S. Chinn, and M.H. Alford. 2011. Internal wave climates of the Philippine seas. *Oceanography* 24(1):100–111.

Haley, P.J. Jr., and P.F.J. Lermusiaux. 2010. Multiscale two-way embedding schemes for free-surface primitive equations in the Multidisciplinary Simulation, Estimation and Assimilation System. *Ocean Dynamics* 60:1,497–1,537, doi:10.1007/s10236-010-0349-4.

Haley, P.J. Jr., P.F.J. Lermusiaux, A.R. Robinson, W.G. Leslie, O. Logoutov, G. Cossarini, X.S. Liang, P. Moreno, S.R. Ramp, J.D. Doyle, and others. 2009. Forecasting and reanalysis in the Monterey Bay/California Current region for the Autonomous Ocean Sampling Network-ii experiment. *Deep Sea Research Part II* 56(3–5):127–148, doi:10.1016/j.dsr2.2008.08.010.

Hodur, R.M. 1997. The Naval Research Laboratory's Coupled Ocean/Atmosphere Mesoscale Prediction System (COAMPS). *Monthly Weather Review* 125(7):1,414–1,430.

Hurlburt, H.E., E.J. Metzger, J. Sprintall, S.N. Riedlinger, R.A. Arnone, T. Shinoda, and X. Xu. 2011. Circulation in the Philippine Archipelago simulated by 1/12° and 1/25° global HYCOM and EAS NCOM. *Oceanography* 24(1):28–47.

Ingleby, B., and M. Huddleston. 2007. Quality control of ocean temperature and salinity profiles: Historical and real-time data. *Journal of Marine Systems* 65:158–175, doi:10.1016/j.jmarsys.2005.11.019.

Jackson, C.R., Y. Arvelyna, and I. Asanuma. 2011. High-frequency nonlinear internal waves around the Philippines. *Oceanography* 24(1):90–99.

Jones, B.H., C.M. Lee, G. Toro-Farmer, E.S. Boss, M.C. Gregg, and C.L. Villanoy. 2011. Tidally driven exchange in an archipelago strait: Biological and optical responses. *Oceanography* 24(1):142–155.

Lam, F.P, P.J. Haley Jr., J. Janmaat, P.F.J. Lermusiaux, W.G. Leslie, M.W. Schouten, L.A. te Raa, and M. Rixen. 2009. At-sea real-time coupled four-dimensional oceanographic and acoustic forecasts during battlespace preparation 2007. In special issue on "Coastal Processes: Challenges for Monitoring and Prediction," J.W. Book, M. Orlic, and M. Rixen, eds. *Journal of Marine Systems* 78:S306–S320, doi:10.1016/j.jmarsys.2009.01.029.

Leben, R.R., G.H. Born, and B.R. Engebreth. 2002. Operational altimeter data processing for meso-scale monitoring. *Marine Geodesy* 25:3–18.

Locarnini, R.A., A.V. Mishonov, J.I. Antonov, T.P. Boyer, and H.E. Garcia. 2006. *World Ocean Atlas 2005. Volume 1: Temperature.* S. Levitus, ed., NOAA Atlas NESDIS 61, US Government Printing Office, Washington, DC, 182 pp.

Lermusiaux, P.F.J. 1999. Data assimilation via error subspace statistical estimation. Part II: Middle Atlantic bight shelfbreak front simulations and ESSE validation. *Monthly Weather Review* 127(8):1,408–1,432.

Lermusiaux, P.F.J. 2002. On the mapping of multi-variate geophysical fields: Sensitivity to size, scales and dynamics. *Journal of Atmospheric and Oceanic Technology* 19(10):1,602–1,637.

Lermusiaux, P.F.J. 2006. Uncertainty estimation and prediction for interdisciplinary ocean dynamics. In special issue on "Uncertainty Quantification," J. Glimm and G. Karniadakis, eds. *Journal of Computational Physics* 217(1):176–199.

Lermusiaux, P.F.J. 2007. Adaptive sampling, adaptive data assimilation and adaptive modeling. In special issue on "Mathematical issues and challenges in data assimilation for geophysical systems: Interdisciplinary perspectives," C. Jones and K. Ide, eds. *Physica D* 230:172–196.

Lermusiaux, P.F.J., and A.R. Robinson, 2001. Features of dominant mesoscale variability, circulation patterns and dynamics in the Strait of Sicily. *Deep Sea Research Part I* 48(9)1,953–1,997.

Lermusiaux, P.F.J., D.G.M. Anderson, and C.J. Lozano, 2000. On the mapping of multi-variate geophysical fields: Error and variability subspace estimates. *Quarterly Journal of the Royal Meteorological Society* 126:1,387–1,429.

Lermusiaux, P.F.J., P.J. Haley Jr., W.G. Leslie, O. Logutov, A. Agarwal, and L. Burton. 2009. Real-time IOP09 Multiscale Field Estimation, Forecasting and Dynamical Descriptions. http://mseas.mit.edu/Sea_exercises/Straits/index.html.

Lermusiaux, P.F.J., J. Xu, C.F. Chen, S. Jan, L.Y. Chiu, and Y.-J. Yang, 2010. Coupled ocean-acoustic prediction of transmission loss in a continental shelfbreak region: Predictive skill, uncertainty quantification and dynamical sensitivities. *IEEE Transactions, Journal of Oceanic Engineering* 35(4)895–916, doi:10.1109/JOE.2010.2068611.

Logutov, O.G. 2008. A multigrid methodology for assimilation of measurements into regional tidal models. *Ocean Dynamics* 58:441–460, doi:10.1007/s10236-008-0163-4.

Logutov, O.G., and P.F.J. Lermusiaux. 2008. Inverse barotropic tidal estimation for regional ocean applications. *Ocean Modelling* 25:17–34, doi:10.1016/j.ocemod.2008.06.004.

May, P.W., J.D. Doyle, J.D. Pullen, and L.T. David. 2011. Two-way coupled atmosphere-ocean modeling of the PhilEx Intensive Observational Periods. *Oceanography* 24(1):48–57.

Metzger, E.J., and H.E. Hurlburt. 1996. Coupled dynamics of the South China Sea, the Sulu Sea, and the Pacific Ocean. *Journal of Geophysical Research* 101(C5):12,331–12,352.

MSEAS Group. 2010. *The Multidisciplinary Simulation, Estimation, and Assimilation Systems* [MSEAS] (http://mseas.mit.edu/, http://mseas.mit.edu/codes). Reports in Ocean Science and Engineering 6, Department of Mechanical Engineering, MIT, Cambridge, Massachusetts.

Ohlmann, J.C. 2011. Drifter observations of small-scale flows in the Philippine Archipelago. *Oceanography* 24(1):122–129.

Pullen, J.D., A.L. Gordon, J. Sprintall, C.M. Lee, M.H. Alford, J.D. Doyle, and P.W. May. 2011. Atmospheric and oceanic processes in the vicinity of an island strait. *Oceanography* 24(1):112–121.

Qu, T., and R. Lukas. 2003. The bifurcation of the North Equatorial Current in the Pacific. *Journal of Physical Oceanography* 33:5–18.

Quadfasel, D., H. Kudrass, and A. Frische. 1990. Deep-water renewal by turbidity currents in the Sulu Sea. *Nature* 348:320–322.

Rosenthal, Y., D.W. Oppo, and B.K. Linsley. 2003. The amplitude and phasing of climate change during the deglaciation in the Sulu Sea, western equatorial Pacific. *Geophysical Research Letters* 30(8):16, doi:10.1029/2002GLO16612.

Rosmond, T.E. 1992. The design and testing of the Navy Operational Global Atmospheric Prediction System. *Weather and Forecasting* 7(2):262–272.

Rypina, I., L. Pratt, J. Pullen, J. Levin, and A. Gordon. 2010. Chaotic advection in an archipelago. *Journal of Physical Oceanography* 40:1,988–2,006, doi:10.1175/2010JPO4336.1.

Smith, W.H.F., and D.T. Sandwell. 1997. Global seafloor topography from satellite altimetry and ship depth soundings. *Science* 277:1,957–1,962.

Tessler, Z.D., A.L. Gordon, L.J. Pratt, and J. Sprintall. 2010. Transport and dynamics of the Panay sill overflow in the Philippine seas. *Journal of Physical Oceanography*, doi:10.1175/2010JPO4395.1.

Tian, R.C., P.F.J. Lermusiaux, J.J. McCarthy, and A.R. Robinson. 2004. A generalized prognostic model of marine biogeochemical-ecosystem dynamics: Structure, parameterization and adaptive modeling. *Harvard Reports in Physical/Interdisciplinary Ocean Science* 67:1–65.

Ueckermann, M.P. 2009. Towards Next Generation Ocean Models: Novel Discontinuous Galerkin Schemes for 2D unsteady biogeochemical models. Master's Thesis, Massachusetts Institute of Technology, Department of Mechanical Engineering, September 2009.

Villanoy, C.L., O.C. Cabrera, A. Yñiguez, M. Camoying, A. de Guzman, L.T. David, and P. Flament. 2011. Monsoon-driven coastal upwelling off Zamboanga Peninsula, Philippines. *Oceanography* 24(1):156–165.

Vitousek, S., and O.B. Fringer. 2010. Physical vs. numerical dispersion in nonhydrostatic ocean modeling. *Ocean Modelling*, submitted.